 Published version: https://dx.doi.org/10.1088/2057-1976/aaeb65

Synchrotron-based phase contrast imaging of cardiovascular tissue in mice – grating interferometry or phase propagation?

Bram Trachet, PhD[1,2], Goran Lovric, PhD[3,4], Pablo Villanueva-Perez, PhD[4], Lydia Aslanidou[1], Mauro Ferraro, PhD[1], Gerlinde Logghe[2], Nikolaos Stergiopulos, PhD[1] and Patrick Segers, PhD[2]

[1] Institute of Bioengineering, Ecole Polytechnique Federale de Lausanne, Lausanne, Switzerland

[2] bioMMeda, Ghent University, Ghent, Belgium

[3] Centre d'Imagerie BioMédicale, École Polytechnique Fédérale de Lausanne, Lausanne, Switzerland

[4] Swiss Light Source, Paul Scherrer Institute, Villigen, Switzerland

E-mail: bram.trachet@epfl.ch

Abstract

Synchrotron-based X-ray phase-contrast imaging allows for detailed 3D insight into the microstructure of soft tissue and is increasingly used to improve our understanding of mouse models of cardiovascular disease. Two techniques dominate the field: grating interferometry, with superior density contrast at mid to lower microscopic resolutions, and propagation-based phase contrast, facilitating high-resolution tissue imaging. The choice between these techniques depends on which features one is interested in visualizing and is thus highly sample-dependent. In this manuscript we systematically evaluate the advantages and disadvantages of grating interferometry and propagation-based phase contrast on samples obtained from 5 different mouse models of cardiovascular disease, ranging from carotid plaques over ascending and abdominal aortic aneurysms to hypertrophic hearts. Based on our findings we discuss in detail how synchrotron-based imaging can be used to increase our understanding of the anatomy and biomechanics of cardiovascular disease in mice. We also present a flowchart that can help future users to select the best synchrotron-based phase contrast technique for their pre-clinical cardiovascular samples.

Keywords: synchrotron-based X-ray imaging, grating interferometry, phase propagation, mouse models of cardiovascular disease

1. Introduction

Cardiovascular disease is the major cause of death in the Western world [1]. Pre-clinical cardiovascular research, often driven by genetic or pharmacological mouse models [2, 3], allows researchers to gain mechanistic insight into the initiation, progression and ruptures of plaques, aneurysms or dissections without risking human lives. Due to their small size and fast heartbeat, cardiovascular imaging in these mice typically requires a much higher resolution than what is the state-of-the-art in a clinical setting. In recent years, synchrotron-based phase-contrast imaging has emerged as a promising high-resolution technique that can outperform the resolutions achieved by traditional pre-clinical imaging techniques [4]. As opposed to traditional micro-CT, where the images are created based on differing absorption of X-rays that travel through an inhomogeneous specimen, phase-contrast imaging visualizes phase distortions in the X-ray wave fronts that travel through a specimen. Taking advantage of the elastic interactions of the X-rays rather than their inelastic interactions (as is the case for absorption), phase-contrast imaging generally allows for better signal to noise ratios and/or improved spatial resolutions for biological tissue in the hard X-ray domain [5].

Such drastic improvements in image quality can affect the state-of-the-art in many, often unsuspected ways. One potentially disruptive aspect is that of cardiovascular computational biomechanics. The current state of the art in that field is limited by the lack of accuracy in the 3D imaging methods that are needed to create the models [6, 7]. Despite the fact that more and more evidence emphasizes the importance of the micro-structure in disease initiation and

progression [8], computational models typically model both the aortic wall and the aortic thrombus as homogeneous structures without taking the micro-structure into account [9]. We have recently started to exploit the potential of synchrotron-based biomechanics in order to overcome the limitations imposed by traditional imaging methods [10], but the potential of synchrotron-based micro-structural computational models still remains to be explored. Phase contrast synchrotron imaging has also been used to relate locally disturbed hemodynamics to plaque location [11, 12] and to show that intercostal and other minor side branches play an important and previously undetected role in the initiation of dissecting aneurysm in mice [13, 14]. Even research on the largest cardiovascular structure, the heart, can benefit from a shift in perspective: synchrotron-based phase contrast imaging was recently used to obtain detailed volumetric measurements of the anatomical changes that occur during distinct developmental stages of the heart in mouse embryos [4]. In summary, synchrotron-based imaging has only just started to affect the field of pre-clinical cardiovascular research.

For researchers who want to exploit the possibilities offered by phase-contrast synchrotron imaging in order to investigate their cardiovascular samples, it is very important to select the imaging technique that best fits their application. In this manuscript we focus on three specific synchrotron-based phase contrast imaging techniques: grating-based interferometry [15], propagation-based phase contrast without phase retrieval and propagation-based phase contrast in combination with a single-distance phase-retrieval algorithm [16]. In grating interferometry, the X-ray phase signal is extracted from the change in the phase stepping curve with and without sample [5]. In propagation-based phase-contrast without phase retrieval the recorded images are equivalent to the ones obtained in traditional absorption micro-CT, albeit with the additional enhancement of the edges at different matter interfaces. In propagation-based phase-contrast with phase retrieval, edge-enhanced fringes are exploited in algorithms to retrieve the X-rays phase shift induced by the object which is proportional to the electron density [17]. A quantitative comparison was carried out by Lang *et al*. [18] and Zanette *et al* [19], who both used tissue from an adult rat, and by Holme *et al* [20], who used tissue of human coronary arteries. These authors concluded that (i) grating interferometry and phase propagation are complementary techniques, (ii) grating interferometry is more complex than phase propagation but yields better density resolution at the cost of a more coarse resolution, and (iii) the optimal choice of imaging technique strongly depends on the sample that is being investigated.

Such sample-specific requirements are, however, not always easy to identify. Since the characteristic lengths and tissue densities can vary significantly in between different species, results obtained in cardiovascular tissue from humans or rats are not necessarily representative for mice. Even within the same species, the requirements are very different for a narrowed carotid artery than for a dilated abdominal aorta. Nevertheless, and despite the fact that mouse models are our first and foremost source of insight into the initiation and propagation of cardiovascular disease, there are currently no comparative studies that focus on the trade-off between contrast-to-noise ratio and resolution for synchrotron-based phase contrast imaging of cardiovascular tissue in mice. This manuscript aims to close that gap in literature through an experimental comparison of grating-based and phase propagation-based contrast imaging that focuses solely on murine cardiovascular tissues. A wide range of healthy and diseased murine samples was investigated, with critical voxel sizes ranging from the carotid artery (diameter: 0.5 mm) over the aneurysmal aorta (diameter: 2-3 mm) to the hypertrophic heart (diameter: 12 mm). We systematically assessed the contrast-to-noise ratio (CNR) and the spatial resolution from a user point of view, thus providing a generalized image quality evaluation with two figures of merit. For some samples (e.g. mouse hypertrophic heart) the images presented in this paper are the first synchrotron images that have been made in these tissues.

2. Materials and Methods

2.1 Animal models

Modif. gene	Cardiovasc disease	Method	Field of view	Feature of interest	Priority
ApoE$^{-/-}$	Carotid plaque	Vasc. cast	0.5x0.5 mm	Thrombus	CNR
THSD 4	Hypertr. heart	/	12x12 mm	Micro-structure	Resol.
ApoE$^{-/-}$	Ascending aneurysm	Ang II + BAPN	2x2 mm	Micro-structure	Resol.
ApoE$^{-/-}$	Dissecting aneurysm	Ang II + BAPN	3x3 mm	Micro-structure + thrombus	Resol. + CNR
/	Abdomin. aneurysm	Elastase + anti-TGF-β	3x3 mm	Micro-structure + thrombus	Resol. + CNR

Table 1. ***Cardiovascular mouse models and sample characteristics.***

In accordance with the 3R principle (replacement, reduction, refinement) all animal tissues were reused from ongoing studies. A summary of the cardiovascular samples that were used is presented in Table 1, along with their relevant features. Representative 3D images of the samples (segmented in Mimics (Materialise, Leuven, Belgium) based on images from grating interferometry) are shown in Figure 1. N=1 carotid plaque was induced in the carotid artery of an atherosclerotic ApoE$^{-/-}$ mouse via flow manipulation by a perivascular collar [21] and compared to a healthy carotid artery from an C57Bl/6 mouse. N=2 hypertrophic hearts were obtained from mice with a mutation in the ADAMTS-like 6 protein (THSD4) that promotes the fibrillin-1 microfibril assembly. N=2 abdominal aortic aneurysms (AAAs) were induced into a C57Bl/6J mouse by a combination of peri-adventitial elastase with TGFβ neutralization. N=2 dissecting aortic aneurysms and n=2 ascending aortic aneurysms were induced in 4 different

animals by a combination of angiotensin II (Ang II) infusion and β-aminopropionitrile monofumarate (BAPN)[22].

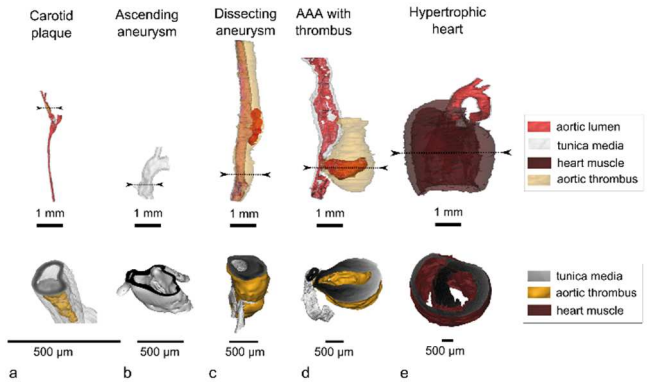

Fig. 1. ***Representative 3D images of the 5 cardiovascular samples.*** *The upper row shows a 3D image of the full sample. The clipping plane that is shown in the lower row is indicated with a dashed line. For reasons of uniformity all 3D images were segmented based on images obtained with grating interferometry. Note that the scale bar in upper panels is uniform for all samples (1mm), while the lower panels have been scaled to allow for a better visualization of the feature of interest.*

All procedures were approved by the Ethical Committee of the respective institutions (carotid plaque: Erasmus MC, Rotterdam, Holland; hypertrophic hearts: Shriners hospital, Portland, United States; abdominal aneurysm: Cambridge University, Cambridge, United Kingdom; dissecting aneurysm: Kurume University, Fukuoka, Japan) and performed according to the guidelines from Directive 2010/63/EU of the European Parliament on the protection of animals used for scientific purposes. After sacrifice, all tissues were carefully excised and samples were fixed by immersion in freshly prepared 4% paraformaldehyde (PFA) at 4°C temperature for 24 hours.

2.2 Imaging setup

The experiments were carried out at the X02DA TOMCAT beamline of the Swiss Light Source (SLS) at the Paul Scherrer Institute (Villigen, Switzerland). The X-ray beam, produced by a 2.9 T bending magnet on a 2.4 GeV storage ring (with ring current I = 400 mA, top-up mode), was monochromated with a double-multilayer monochromator. Imaging was performed at two different endstations (Fig. 2). In endstation I, propagation-based phase-contrast microtomography was performed at 25m source-to-sample distance, 25 cm sample-to-detector distance and at 21 keV. A scientific CMOS detector (pco.Edge 5.5) was used in combination with a 4x magnifying (UPLAPO4x) visible-light optics and a 20 µm thick scintillator. The effective pixel size was 1.625 x 1.625 µm^2. In endstation II, grating-based phase-contrast microtomograhy was performed at 30 m source-to-sample and at 25 keV.

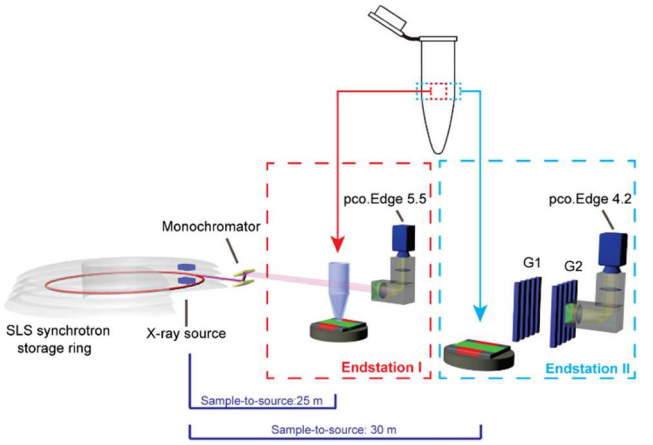

Fig. 2. ***The experimental setup with two different endstations.***

Phase retrieval was based on single defocused images using a transport-of-intensity approximation as originally proposed by Paganin *et al.* [16, 23]. A grating interferometer was mounted right after the sample and consisted of a phase grating (G1) with a pitch of 4 µm and an absorption grating (G2) with a 2 µm pitch positioned at a distance corresponding to the third Talbot order [33]. The detector used in the grating interferometry setup was a scientific CMOS detector (pco.Edge 4.2) in combination with 1:1 magnifying visible light optics and a 300 µm thick scintillator, yielding an effective pixel size of 6.5 x 6.5 µm^2. Each tissue was imaged sequentially with propagation-based phase-contrast imaging on endstation I and with grating-based phase-contrast imaging on endstation II.

2.3 Image analysis

For each cardiovascular application one severe and one moderate phenotype was selected. This resulted in one carotid artery with plaque and one without, one dissecting aneurysm with intramural hematoma and one without, one end-stage ascending aneurysm with a large medial tear and one with only micro-ruptures, one abdominal aneurysm with large intraluminal thrombus and one without thrombus, and two hypertrophic hearts of different sizes (Table 1, Fig. 1). Each of these 10 samples was studied with the three aforementioned different imaging methods, and for each of these 30 scans we selected 4 representative images from the stack that represented healthy, intermediate and diseased regions of the vessel/heart. This resulted in a set of 120 images for which we analyzed the contrast-to-noise ratio (CNR), the spatial resolution and the trade-off between spatial resolution and image contrast. The resolution was determined by taking a line profile in the middle of the image and calculating its power spectral density (PSD). The converged value of the PSD at the noise baseline was subsequently doubled and matched to the respective spatial frequency [24]. The resolution x_{res} was calculated by:

$$x_{res} = p_{size} \frac{x_n}{k_{res}} \quad (1)$$

where p_{size} is the pixel size of the detector, x_n the number of pixels for the taken line profile and k_{res} the pixel frequency obtained from the resolution criterion. For the calculation of CNR the following formula was used [25]:

$$CNR = 2\left(\frac{|S_{obj} - S_{bg}|}{\sigma_{obj} + \sigma_{bg}}\right) \quad (2)$$

where S_i and σ_i represent the mean pixel values and corresponding standard deviations of a manually defined region of interest (ROI) representing an object (obj) and a background (bg) region (Fig 3b). Typically, the CNR is defined as the ratio of the contrast to the overall noise level in the image. The formula used here accounts for more general situations where the object and background noises are dissimilar. This is the case when comparing features at different spatial resolutions that have heterogeneous densities. The size of the ROI was fixed at 39x39 µm^2 for all images (corresponding to 6x6 pixels in grating interferometry and 24x24 pixels in phase propagation). Two different object ROIs were chosen for each image and the mean value was reported to mitigate the effect of local variations. The size of the ROI was relatively small with respect to the size of the total image, in order to avoid the presence of structures (signal rather than noise) within the object ROI.

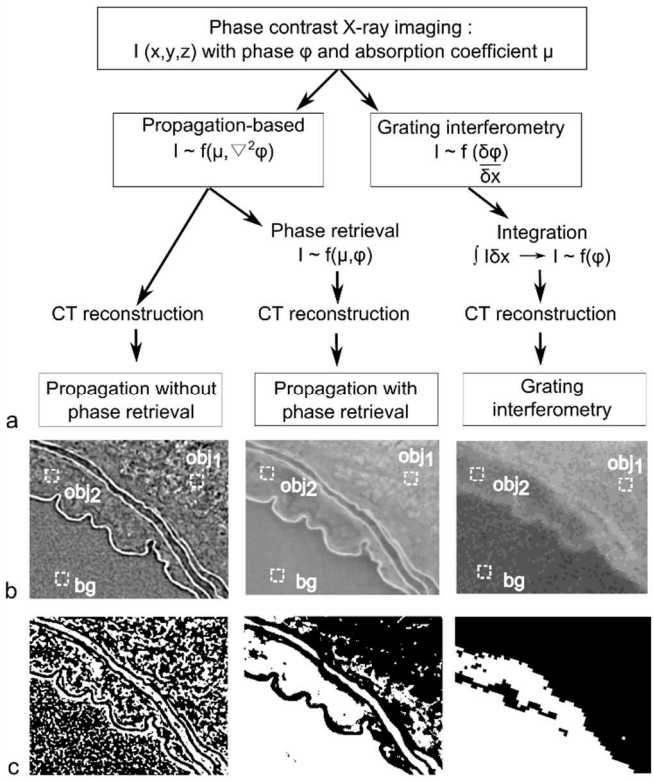

Fig. 3. ***Phase propagation versus grating interferometry***. *(a). Flow chart summarizing the differences between phase propagation techniques and grating interferometry. (b). Representative images of the location of ROIs for background (bg) and object (obj) that were used for CNR calculations. (c). Binary images visualize the difference in segmentation properties between the different images shown in panel b.*

2.4 Statistics

All data were tested for normality by the Shapiro-Wilk parametric hypothesis test and visually checked for adherence to the x=y reference line on a normal probability plot. Equal variance was tested with Bartlett's test. The conditions for parametric testing were met in all cases and the differences between imaging techniques were therefore analyzed with a one-way Anova analysis. Post-hoc pairwise comparisons were performed using a Bonferroni correction. A p-value < 0.05 was considered significant (*), and a p-value < 0.001 was considered highly significant (**). All values are reported as mean ± standard deviation.

3. Results

3.1 Quantitative assessment of resolution and CNR

	Unit	Phase prop. (no phase retrieval)	Phase prop. with phase retrieval	Grating Interferom.
Energy	keV	21	21	25
Acquis. time	s	270	270	1350
Field of View	mm x mm	4.2 x 4.2	4.2 x 4.2	12.7 x 12.7
Pixel size	µm	1.625	1.625	6.5
Resol.	µm	4.1 ± 0.1	5.0 ± 1.3	13.7 ± 1.3
CNR	/	0.17 ± 0.14	2.9 ± 3.1	12.3 ± 10.1

Table 2. ***Imaging settings and resulting image quality parameters for cardiovascular samples obtained from mice.***

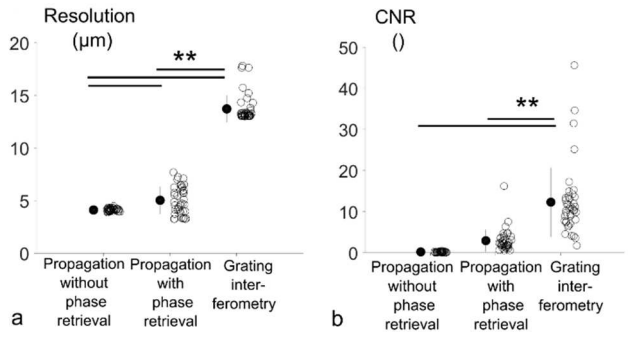

Fig 4. ***Differences in resolution and CNR between the 3 different imaging techniques.***

The resolution of grating interferometry was consistently and significantly coarser than the resolution of propagation-based techniques (Table 2, Fig. 4). The difference in resolution between phase propagation with and without phase retrieval was also statistically significant (Fig. 4a). The CNR was found to be consistently and significantly higher for grating interferometry than for both propagation-based approaches (Fig. 4b), while the difference in CNR between phase propagation with and without phase reconstruction was borderline significant (p=0.057).

3.2 Qualitative assessment of relevant cardiovascular features

While both phase propagation methods resolve the lamellae that make up the aortic wall in the carotid, ascending and abdominal aorta, the aortic wall appears as a homogeneous entity when the same tissues are scanned with grating interferometry (Fig 5a-5e). In the ascending aneurysm, phase propagation allows for the visualization of micro-ruptures in the lamellae that are not visible with grating interferometry (Fig 5b, arrows). Indeed, aortic lamellae are 4-10 micrometer thick and are thus sub-resolution for grating interferometry (13.7 µm) but not for phase propagation with (5.0 µm) or without phase retrieval (4.1 µm).

3.3 Sample-specific comparison

Another immediate observation is the difference in image contrast. The transition from carotid plaque to carotid lumen is clearly visible on both phase propagation images, but not on grating interferometry (Fig 5a, arrows). The contrast between different layers within the aneurysm thrombus, on the other hand, is clearly visible in grating interferometry and phase propagation with phase retrieval, but not in phase propagation without phase retrieval (Fig 5e, arrows). This is consistent with the binary images of a dissecting aneurysm (Fig 3c):

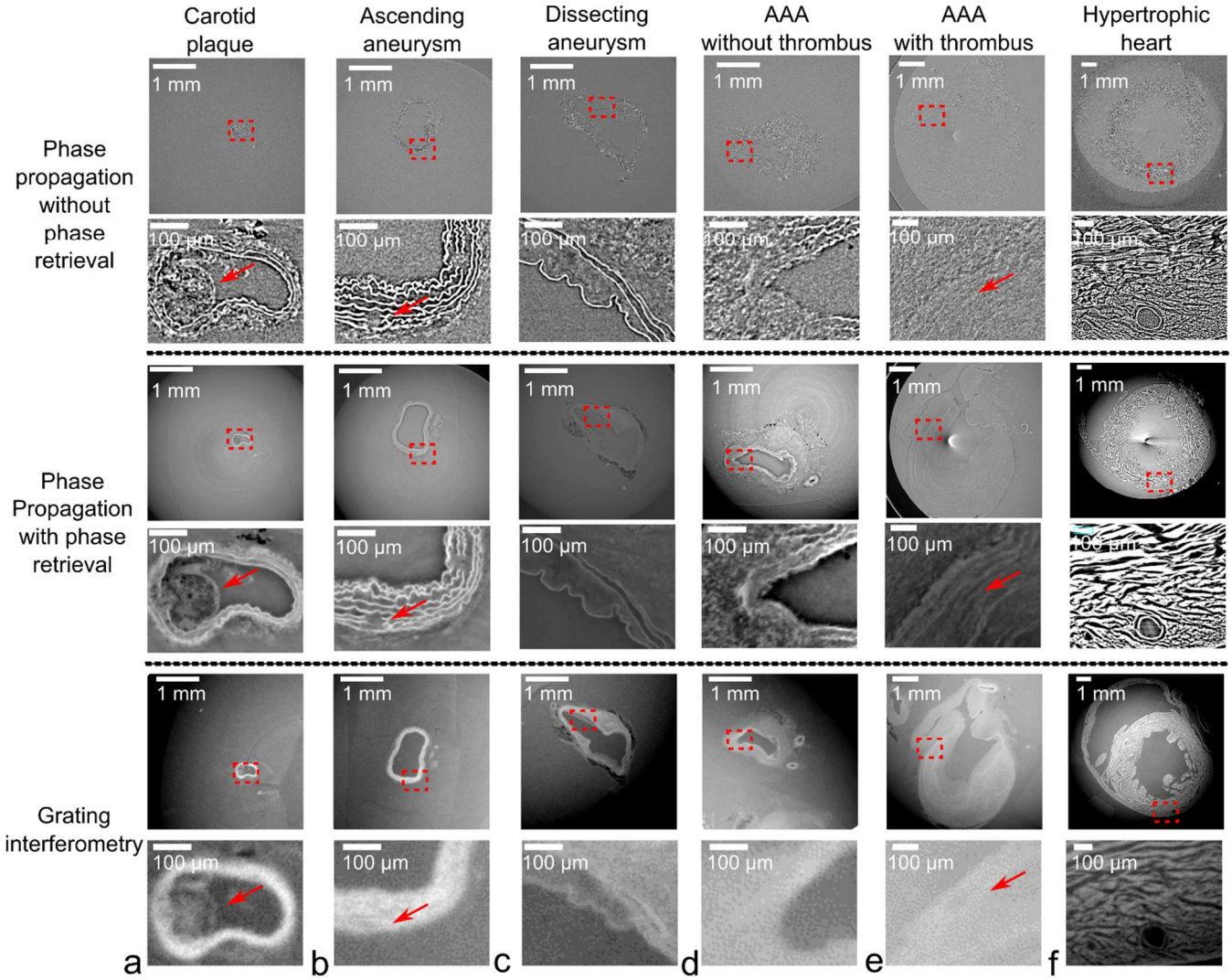

Fig 5. ***Representative 2D images of the three imaging techniques and the 5 cardiovascular samples****. For each imaging technique the upper row shows a 2D image of the full sample, while the ROI that was used for the zoomed image in the lower row is indicated with a red rectangle. Arrows indicate carotid plaque (a), lamellar rupture (b) and layered architecture of the thrombus (e). Note that the scale bar in panels e and f s is smaller, since these samples were larger.*

grating interferometry results in a sharp and homogeneous contrast between the thrombus (in black, upper right quadrant) and the lumen (in white, lower left quadrant) while phase propagation without phase retrieval results in a scattered, almost random distribution of pixels in both zones. When phase retrieval is applied, phase propagation results in better segmentability, but without achieving the level of contrast obtained by grating interferometry (Fig 3c).

A sample-specific comparison of the resolution and CNR for each of the three imaging techniques revealed significant differences between samples (Fig. 6). For images obtained without phase retrieval the smallest resolution was observed in the carotid artery (Fig. 6a), while the ascending and AAA samples had the coarsest resolution when phase propagation with phase retrieval was used (Fig. 6b). The resolution of the hearts was significantly coarser than the resolution of the other samples when using grating interferometry (Fig 6c). For the images obtained with phase propagation no sample-specific differences in CNR could be observed (Fig 6d, 6e). The CNR of the AAA and the heart was slightly higher than the CNR of the other samples when using grating interferometry (Fig 6f), but the difference did not reach significance.

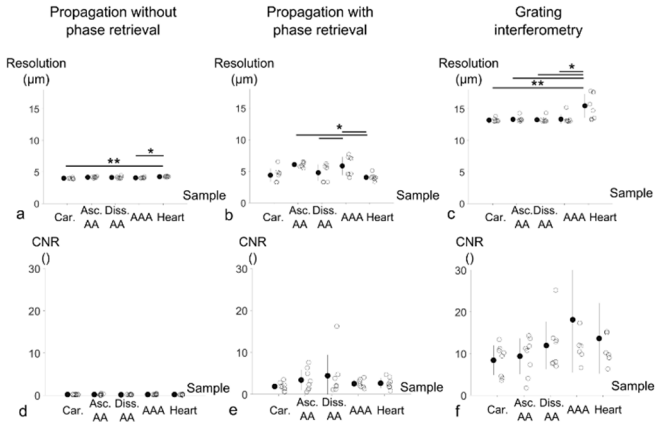

Fig 6. ***Sample-specific comparison of resolution and CNR.***

4. Discussion

4.1 Sample-specific guidelines

In order to translate our results into practical guidelines for future users who want to perform synchrotron-based phase contrast imaging of cardiovascular tissue, we have condensed our findings in a flowchart (Fig. 7). Depending on the sample-specific requirements, three different outcomes are possible.

4.1.1 Focus on discrete micro-structural elements within the cardiovascular tissue (e.g. aortic lamellae)

If the application requires the user to quantify discrete, non-homogeneous micro-structures (in our case voxel sizes between 4x4x4 and 14x14x14 µm^3), one should optimize for resolution rather than CNR [26]. In this case the best choice is to use phase propagation without phase retrieval. The dense spatial resolution of these phase propagation images allows for the visualization of micro-structures that cannot be resolved with grating interferometry. This is for example the case for aortic lamellae in the tunica media of the aortic wall (Fig. 5b). These lamellae are also visible when phase propagation with phase retrieval is used, albeit at a slightly worse resolution. This is likely due to the fact that the phase reconstruction algorithm acts as a low pass filter, which enhances the contrast but slightly reduces the achievable resolution [16].

4.1.2 Focus on continuous macro-structural elements within the cardiovascular tissue (e.g. thrombus)

If the application requires the user to differentiate between adjacent, continuous regions that are expected to have a different pixel density [27] , one should optimize for CNR rather than resolution. This is the case for users that want to get a detailed visualization of e.g. a thrombus that formed within an aneurysm or a plaque. If the ROI is sufficiently large (see below), grating interferometry is the method of choice in this case. Indeed, the high value of CNR that is achieved by grating interferometry is an indication for good pixel homogeneity within the ROI that was used to define the object region (Fig 4b, 3c).

4.1.3 Focus on both micro-and macrostructural elements at the same time (e.g. aortic plaque)

If the application requires the user to get the best possible images of both discrete micro-structural elements and continuous macro-structural elements [13], one should try to find the best possible compromise between CNR and resolution. As soon as the size of the smallest homogeneous ROI is smaller than 40 µm^3, which is e.g. the case for carotid plaque, phase propagation with phase retrieval should be the method of choice. The cut-off value of 40x40x40µm^3 corresponds to the size of the ROI that was used to determine the CNR, i.e. 6x6 pixels in grating interferometry and 24x24 pixels in phase propagation. For smaller ROIs, grating interferometry at TOMCAT is hampered by its limited resolution. For larger ROIs, the user will have to balance resolution and CNR according to his/her personal needs. If the image should above all be easily segmentable, grating interferometry will be the method of choice. The same is true for large samples that don`t fit in the smaller field of view of phase propagation imaging. If, on the other hand, as many sub-structures as possible should be resolved, phase propagation with phase retrieval will yield better results. The reason for the latter is that the high CNR of grating interferometry can in

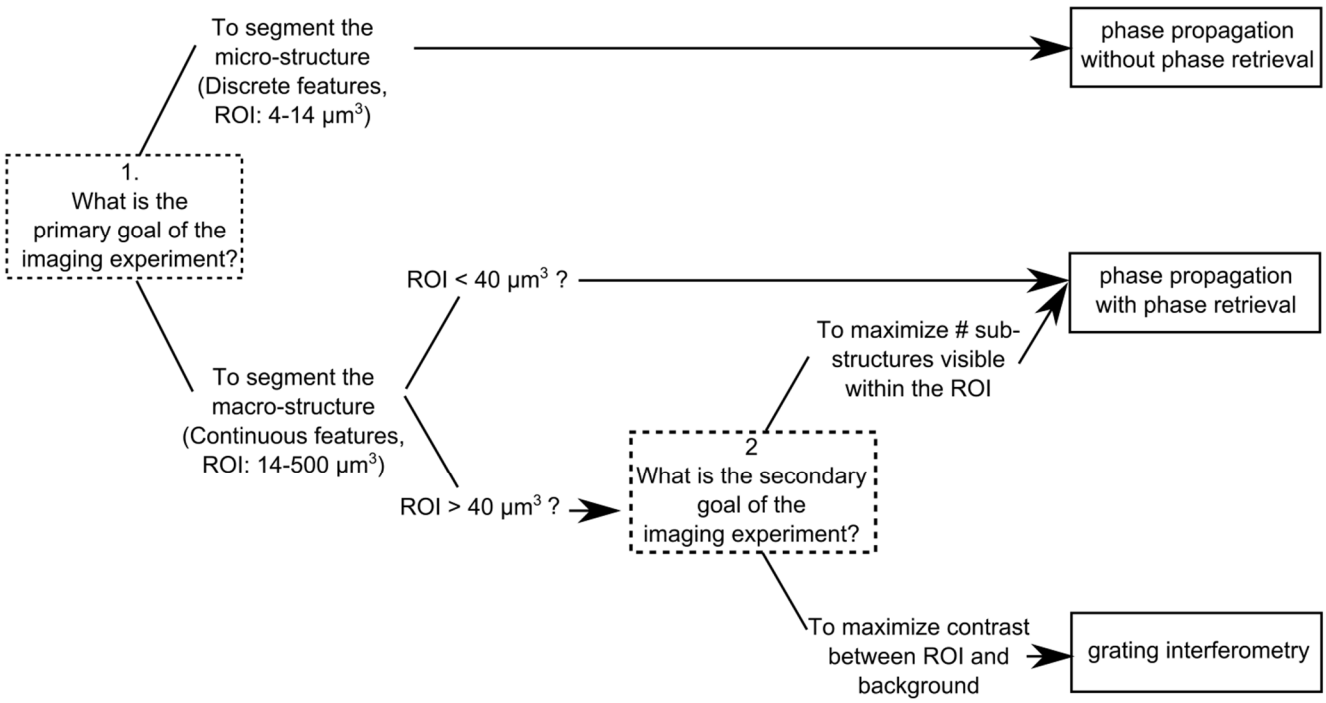

Fig 7. ***Flowchart to help future synchrotron users deciding which phase contrast technique is most appropriate to scan pre-clinical cardiovascular samples.***

some cases mask the heterogeneity of the underlying cardiovascular tissue (i.e. the signal, not the noise). If the underlying tissue is not actually homogeneous but cannot be resolved due to the limited resolution of the technique (which is e.g. the case for the aortic wall), grating interferometry will result in an artificially homogeneous yet easily segmentable image (Fig. 3c).

4.2 Phase-contrast imaging and pre-clinical cardiovascular research

From carotid plaques to hypertrophic hearts, synchrotron-based phase contrast imaging has the potential to bring new insights into the field of cardiovascular imaging. An important prerequisite is that the proper technique be used for each applications. The overview presented in Figure 7 can serve as a guideline to help future synchrotron users decide which technique best fits their cardiovascular sample. It can, however, also be used to re-interpret some of the already published results in literature.

Several researchers have used grating interferometry to study mouse coronary or carotid plaques [28, 29]. While this technique can indeed be used to contrast the plaque region from the lumen surrounding it, the flowchart presented in Figure 7 clearly shows that propagation-based techniques would have allowed for sufficient CNR at a higher resolution. Assemat *et al.* used propagation-based synchrotron images with phase retrieval as the basis of their biomechanical models of carotid plaque in the mouse aortic arch [11]. Indeed, when phase propagation with phase retrieval is used the inhomogeneities within the plaque thrombus, as well as the plaque thickness, can be visualized in much more detail than what is possible with grating interferometry (Figure 5a). This, in turn, allows for a more accurate assessment of plaque vulnerability and allows to assess the risk of myocardial infarction (in the coronary arteries) or stroke (in the carotid arteries).

A similar observation can be made for synchrotron-based research on mid-sized cardiovascular diseases such as aortic aneurysm and dissection. In the past we have used grating interferometry to visualize the 3D structure of aortic aneurysms in the ascending aorta of mice [26]. We quantified the size of localized ruptures within the ascending aortic wall and correlated their size to the size of the aneurysms in vivo (as measured by contrast-enhanced micro-CT). We also published two different studies in which we used grating interferometry to study the initiation and propagation of dissecting aortic aneurysms in mice [13, 14]. Grating interferometry did not, however, allow us to resolve the lamellar layers separately in any of these studies. With the benefit of hindsight, phase propagation without phase retrieval would have been a better choice for each of these studies. In the ascending aorta, the superior resolution of phase-propagation imaging would have allowed for 3D insight into the failures of the micro-structure that led to the dilatation of the aorta (Figure 5b). In the abdominal aorta, the improved resolution would have allowed us to visualize the effect of a failing micro-structure (lamellae ruptures near side branches, Figure 5c), while its reasonable performance in terms of CNR would have allowed us to relate these micro-ruptures to the subsequent aberrations in macro-structure (intramural thrombus forming between media and adventitia, Figure 5e). This is why in our most recent publications we used phase

propagation with phase retrieval to visualize the micro-structure within the aortic media (i.e. aortic lamellae) of ascending aortic aneurysms [30] and abdominal aortic aneurysms [31]. These studies were among the first to quantify the damage to the micro-structure of the aortic wall in these diseases, reaching in-plane resolutions similar to what can be achieved with 2D histology along the entire length of the vessel. However, the results presented in the current manuscript clearly show that phase propagation without phase retrieval has a slightly better performance that phase propagation with phase retrieval in terms of resolution (Table 2, Figure 4a). Phase propagation without phase retrieval would thus have been the better choice for both of the aforementioned studies, since they focused on the discontinuous micro-structure and not so much on the difference in density between adjacent regions. Future researchers who want to study aneurysms or dissections in mice should therefore weigh the importance of lamellar discontinuities (better studied without phase retrieval) versus the need to contrast the aortic thrombus from the aortic lumen (better studied with phase retrieval or grating interferometry).

4.3 Limitations and future work

The most important limitation of this work is that our samples were only scanned at a single beamline (TOMCAT, at the Swiss Light Source synchrotron of the Paul Scherrer Institute in Villigen, Switzerland), using a single and optimized set of imaging parameters. Consequently, the comparison presented in this manuscript does not claim to cover the entire state-of-the-art of phase propagation imaging, or even of the TOMCAT beamline. All grating interferometry images in this study were taken with a distance corresponding to the third Talbot order. For samples that require higher sensitivity but not necessarily a better spatial resolution, imaging could be performed at higher order Talbot distances. This may further improve the grating interferometry images of e.g. heart tissue, but would not significantly affect the conclusions of our work. Similarly, all phase propagation images were taken at a 4x magnification, which corresponds to a pixel size of 1.625 µm. Choosing a 10x magnification, a pixel size of 0.65 µm could be achieved. Following this approach a spatial resolution of 1.5-2 μm^3 should be possible when keeping all other imaging parameters constant. It is, however, important to keep in mind that in this case the field of view would reduce accordingly, and one will no longer be able to visualize the entire sample within a single scan. A 4x magnification is therefore the best compromise between resolution and field of view for pre-clinical cardiovascular applications – at least when the goal is to scan the entire sample. For similar reasons we did not vary exposure times or sample-to-detector distances [32], nor did we explore alternative approaches to scan larger samples, such as free space propagation [33]. Additional experiments, performed at TOMCAT or other beamlines around the world, would have allowed us to propose a more complete set of guidelines including (i) a broader scope of sample sizes and (ii) more specific parameter settings. But it is important to keep in mind that the aim of this manuscript was not be as complete or as detailed as possible. Instead, we chose to focus on the imaging techniques (and the settings within these techniques) that will be most useful for the specific subgroup of synchrotron users that are interested in scanning pre-clinical cardiovascular samples. The result is a set of robust and practical guidelines that can help future users to make an educated decision, and that is supported by theoretical and experimental predictions [34-36].

CNR was calculated based on object and background ROIs of 39x39 μm^2. This small size was chosen on purpose in order to be able to place the object ROI within a homogeneous region of the tissue, such as the interlamellar region or the thrombus. Larger ROIs would have implied a risk of structures (i.e. signal rather than noise) disturbing the calculated standard deviation within the ROI. Nevertheless, it is possible that in some cases a small structure (e.g. density variations within the thrombus) may have entered part of the ROI and thus affected the measurement. Also, it is important to point out that the calculated CNR was not corrected for flux. Since the pixels in the phase propagation image were smaller, and the total exposure time was shorter, a pixel in a phase propagation image was exposed to a higher flux than a pixel in a grating interferometry image. The standard deviation within a certain ROI of 6x6 pixels in grating interferometry is therefore expected to be lower than the standard deviation within a ROI of 24x24 pixels in phase propagation. For a comparison at the same pixel size, one could chose to bin the phase propagation images 4x4, such that both ROIs would have 6x6 pixels. However, binned phase propagation images are not what future synchrotron users would work with, and would result in an artificially low resolution and an artificially high CNR. Another option could be to redo the grating interferometry experiments using (i) a detector with reduced pixel size and (ii) grating pitches of the order of the pixel size, in order to reach resolutions comparable to those achieved in phase propagation. However, such grating pitches are difficult to produce and are not what a typical user will encounter at the beamline. It is important to keep in mind that the purpose of our comparison was to quantitatively evaluate the image quality from a user perspective, in terms of segmentability at a given spatial resolution. We therefore chose to stick for each technique to the parameter settings that future users are most likely to encounter, and that were judged optimal for the samples that were being investigated.

Vertical stacking has been used along the rotation axis in order to scan long tubular samples such as the aorta. The constraints that limit the field of view (Table 2) are confined to the horizontal, cross-sectional area of the sample. It is also important to remark that both phase propagation methods had a spatial resolution that was slightly worse than the Nyquist criterion of twice the pixel size. For phase propagation with phase retrieval (pixel size: 1.625 µm, resolution: 5.0 ± 1.3 µm) this was related to the low pass filtering that results from Paganins phase retrieval. Grating interferometry, despite having a coarser resolution, sticks closer to the Nyquist criterion. Finally, grating interferometry does not necessarily

have to be performed at a synchrotron, since table-top solutions are available with a pixel size ranging from 6-20 μm [37]. For large samples this may be an additional argument to choose grating interferometry over phase propagation methods.

5. Conclusions

We studied pre-clinical samples of 5 different mouse models of cardiovascular disease with three different synchrotron-based phase contrast imaging techniques. The consistently and significantly higher contrast-to-noise ratio of grating interferometry (resolution: 13.7 ± 1.3 μm, CNR: 12.3 ± 10.1) makes this technique the ideal choice for samples in which the priority is to differentiate large continuous regions of different density, such as aortic thrombus and aortic lumen. If the application requires the visualization of structural elements within the wall, such as aortic lamellae, the consistently and significantly better resolution of propagation-based phase contrast without phase retrieval (resolution: 4.1 ± 0.1 μm, CNR: 0.17 ± 0.14) yields the best results. Finally, phase propagation with phase retrieval (resolution: 5.0 ± 1.3 μm, CNR: 2.9 ± 3.1) is to be preferred when enhanced contrast is needed at the highest possible resolution. This is e.g. the case if one needs to visualize the micro-structure within carotid plaques or if one is interested to study different layers within an aneurysm thrombus. We conclude that, as long as the appropriate techniques are used for each sample, synchrotron-based phase contrast imaging can be a powerful tool to improve our understanding of the initiation and propagation of cardiovascular disease.

Acknowledgements

The authors would like to acknowledge Z. Mallat and M. Clement from Cambridge University (Cambridge, UK), F. Gijsen and R. Xing from Erasmus MC (Rotterdam, Netherlands), M. Renard and J. De Backer from Ghent University (Ghent, Belgium), L. Sakai from Shriners Hospital for Children (Portland, USA) and H. Aoki from Kurume University (Kurume, Japan) for kindly providing the samples that were used in this study. This research was funded by the Swiss National Science Foundation (SNSF, grant CR23I2_163370). Bram Trachet and Gerlinde Logghe are funded by a post-doctoral and doctoral grant of the research foundation Flanders (FWO, grants 12A5816N and 1S26117N).

References

[1] Pagidipati N J and Gaziano T A 2013 Estimating Deaths From Cardiovascular Disease: A Review of Global Methodologies of Mortality Measurement *Circulation* **127** 749-56

[2] Moon A 2008 *Curr. Top. Dev. Biol.*: Academic Press) pp 171-248

[3] Casteleyn C, Trachet B, Van Loo D, Devos D G, Van den Broeck W, Simoens P and Cornillie P 2010 Validation of the murine aortic arch as a model to study human vascular diseases *J. Anat.* **216** 563-71

[4] Dullin C, Ufartes R, Larsson E, Martin S, Lazzarini M, Tromba G, Missbach-Guentner J, Pinkert-Leetsch D, Katschinski D M and Alves F 2017 μCT of ex-vivo stained mouse hearts and embryos enables a precise match between 3D virtual histology, classical histology and immunochemistry *PLOS ONE* **12** e0170597

[5] Weitkamp T, Diaz A, David C, Pfeiffer F, Stampanoni M, Cloetens P and Ziegler E 2005 X-ray phase imaging with a grating interferometer *Opt. Express* **13** 6296-304

[6] Xing R, De Wilde D, McCann G, Ridwan Y, Schrauwen J T C, van der Steen A F W, Gijsen F J H and Van der Heiden K 2016 Contrast-enhanced micro-CT imaging in murine carotid arteries: a new protocol for computing wall shear stress *BioMedical Engineering OnLine* **15** 156

[7] Pedrigi R M, Mehta V V, Bovens S M, Mohri Z, Poulsen C B, Gsell W, Tremoleda J L, Towhidi L, de Silva R, Petretto E and Krams R 2016 Influence of shear stress magnitude and direction on atherosclerotic plaque composition *Royal Society Open Science* **3** 160588

[8] Niestrawska J A, Viertler C, Regitnig P, Cohnert T U, Sommer G and Holzapfel G A 2016 Microstructure and mechanics of healthy and aneurysmatic abdominal aortas: experimental analysis and modelling *Journal of The Royal Society Interface* **13** 20160620

[9] Gasser T C 2016 Biomechanical Rupture Risk Assessment: A Consistent and Objective Decision-Making Tool for Abdominal Aortic Aneurysm Patients *AORTA Journal* **4** 42-60

[10] Ferraro M, Trachet B, Aslanidou L, Fehervary H, Segers P and Stergiopulos N 2018 Should we ignore what we cannot measure? How non-uniform stretch, non-uniform wall thickness and minor side branches affect computational aortic biomechanics in mice. *Ann. Biomed. Eng.* **46** 159-70

[11] Assemat P, Armitage J A, Siu K K, Contreras K G, Dart A M, Chin-Dusting J P and Hourigan K 2014 Three-dimensional numerical simulation of blood flow in mouse aortic arch around atherosclerotic plaques *Appl. Math. Model.* **38** 4175-85

[12] Assemat P, Siu K K, Armitage J A, Hokke S N, Dart A, Chin-Dusting J and Hourigan K 2014 Haemodynamical stress in mouse aortic arch with atherosclerotic plaques: Preliminary study of plaque progression *Computational and Structural Biotechnology Journal* **10** 98-106

[13] Trachet B, Aslanidou L, Piersigilli A, Fraga-Silva R A, Sordet-Dessimoz J, Villanueva-Perez P, Stampanoni M F M, Stergiopulos N and Segers P 2017 Angiotensin II infusion into ApoE-/- mice: a model for aortic dissection rather than abdominal aortic aneurysm? *Cardiovasc. Res.* **113** 1230-42

[14] Trachet B, Fraga-Silva R A, Piersigilli A, Tedgui A, Sordet-Dessimoz J, Astolfo A, Van der Donckt C, Modregger P, Stampanoni M, Segers P and Stergiopulos N 2015 Dissecting abdominal aortic aneurysm in ang II-infused mice: suprarenal branch ruptures and apparent luminal dilatation *Cardiovasc. Res.* **105** 213-22

[15] Momose A, Kawamoto S, Koyama I, Hamaishi Y, Takai K and Suzuki Y 2003 Demonstration of X-Ray Talbot Interferometry *Japanese Journal of Applied Physics* **42** L866

[16] Paganin D, Mayo S C, Gureyev T E, Miller P R and Wilkins S W 2002 Simultaneous phase and amplitude extraction from a single defocused image of a homogeneous object *J. Microsc.* **206** 33-40

[17] Langer M, Cloetens P, Guigay J-P and Peyrin F 2008 Quantitative comparison of direct phase retrieval algorithms in in-line phase tomography *Med. Phys.* **35** 4556-66

[18] Lang S, Zanette I, Dominietto M, Langer M, Rack A, Schulz G, Le Duc G, David C, Mohr J, Pfeiffer F, Müller B and Weitkamp T 2014 Experimental comparison of grating- and propagation-based hard X-ray phase tomography of soft tissue *Journal of Applied Physics* **116** 154903

[19] Zanette I, Lang S, Rack A, Dominietto M, Langer M, Pfeiffer F, Weitkamp T and Müller B 2013 Holotomography versus X-ray grating interferometry: A comparative study *Applied Physics Letters* **103** 244105

[20] Holme M N, Schulz G, Deyhle H, Weitkamp T, Beckmann F, Lobrinus J A, Rikhtegar F, Kurtcuoglu V, Zanette I, Saxer T and Müller B 2014 Complementary X-ray tomography techniques for histology-validated 3D imaging of soft and hard tissues using plaque-containing blood vessels as examples *Nat. Protocols* **9** 1401-15

[21] Cheng C, Tempel D, van Haperen R, van der Baan A, Grosveld F, Daemen M J A P, Krams R and de Crom R 2006 Atherosclerotic lesion size and vulnerability are determined by patterns of fluid shear stress *Circulation* **113** 2744-53

[22] Kurihara T, Shimizu-Hirota R, Shimoda M, Adachi T, Shimizu H, Weiss S J, Itoh H, Hori S, Aikawa N and Okada Y 2012 Neutrophil-Derived Matrix Metalloproteinase 9 Triggers Acute Aortic Dissection *Circulation* **126** 3070-80

[23] Gureyev T, Mohammadi S, Nesterets Y, Dullin C and Tromba G 2013 Accuracy and precision of reconstruction of complex refractive index in near-field single-distance propagation-based phase-contrast tomography *Journal of Applied Physics* **114** 144906

[24] Modregger P, Lübbert D, Schäfer P and Köhler R 2007 Spatial resolution in Bragg-magnified X-ray images as determined by Fourier analysis *physica status solidi (a)* **204** 2746-52

[25] Hendrick R E 2008 *Breast MRI Fundamentals and Technical Aspects*, (New York: Springer) pp 93-111

[26] Trachet B, Piersigilli A, Fraga-Silva R A, Aslanidou L, Astolfo A, Stampanoni M F M, Segers P and Stergiopulos N 2016 Ascending aortic aneurysm in angiotensin II infused mice: Formation, progression and the role of focal dissections *Arterioscler. Thromb. Vac. Biol.* **36** 673-81

[27] Buscema M, Holme M N, Deyhle H, Schulz G, Schmitz R, Thalmann P, Hieber S E, Chicherova N, Cattin P C, Beckmann F, Herzen J, Weitkamp T, Saxer T and Müller B 2014 Grating interferometry-based phase microtomography of atherosclerotic human arteries. In: *SPIE Optical Engineering + Applications*: SPIE) p 12

[28] Bonanno G, Coppo S, Modregger P, Pellegrin M, Stuber A, Stampanoni M, Mazzolai L, Stuber M and van Heeswijk R B 2015 Ultra-high-resolution 3D imaging of atherosclerosis in mice with synchrotron differential phase contrast: a proof of concept study *Scientific Reports* **5** 11980

[29] Shinohara M, Yamashita T, Tawa H, Takeda M, Sasaki N, Takaya T, Toh R, Takeuchi A, Ohigashi T, Shinohara K, Kawashima S, Yokoyama M, Hirata K-i and Momose A 2008 Atherosclerotic plaque imaging using phase-contrast X-ray computed tomography *American Journal of Physiology - Heart and Circulatory Physiology* **294** H1094-H100

[30] Logghe G, Trachet B, Aslanidou L, Villaneuva-Perez P, De Backer J, Stergiopulos N, Stampanoni M, Aoki H and Segers P 2018 Propagation-based phase-contrast synchrotron imaging of aortic dissection in mice: from individual elastic lamella to 3D analysis *Scientific Reports* **8** 2223

[31] Lareyre F, Clément M, Raffort J, Pohlod S, Patel M, Esposito B, Master L, Finigan A, Vandestienne M, Stergiopulos N, Taleb S, Trachet B and Mallat Z 2017 TGFβ (Transforming Growth Factor-β) Blockade Induces a Human-Like Disease in a Nondissecting Mouse Model of Abdominal Aortic Aneurysm *Arterioscler. Thromb. Vac. Biol.*

[32] Kitchen M J, Buckley G A, Gureyev T E, Wallace M J, Andres-Thio N, Uesugi K, Yagi N and Hooper S B 2017 CT dose reduction factors in the thousands using X-ray phase contrast *Scientific Reports* **7** 15953

[33] Zamir A, Arthurs O J, Hagen C K, Diemoz P C, Brochard T, Bravin A, Sebire N J and Olivo A 2015 X-ray phase contrast tomography; proof of principle for post-mortem imaging *The British Journal of Radiology* **89** 20150565

[34] Diemoz P C, Bravin A and Coan P 2012 Theoretical comparison of three X-ray phase-contrast imaging techniques: propagation-based imaging, analyzer-based imaging and grating interferometry *Opt. Express* **20** 2789-805

[35] Diemoz P C, Bravin A, Langer M and Coan P 2012 Analytical and experimental determination of signal-

to-noise ratio and figure of merit in three phase-contrast imaging techniques *Opt. Express* **20** 27670-90

[36] Ruiz-Yaniz M, Zanette I, Sarapata A, Birnbacher L, Marschner M, Chabior M, Olbinado M, Pfeiffer F and Rack A 2016 Hard X-ray phase-contrast tomography of non-homogeneous specimens: grating interferometry versus propagation-based imaging *Journal of Synchrotron Radiation* **23** 1202-9

[37] Arboleda C, Wang Z and Stampanoni M 2014 Tilted-grating approach for scanning-mode X-ray phase contrast imaging *Opt. Express* **22** 15447-58